9-12-2024

Oncostatin M receptor-dependent signaling assessed by RNA sequencing in mouse hematopoietic stem cells.

Logan S Schwartz

Ruth L. Saxl

Timothy M Stearns

Maria Telpoukhovskaia

Jennifer J. Trowbridge

scientific data

Check for updates

OPEN

DATA DESCRIPTOR

Oncostatin M receptor-dependent signaling assessed by RNA sequencing in mouse hematopoietic stem cells

Logan S. Schwartz[1,2], Ruth L. Saxl[1], Tim Stearns[1], Maria Telpoukhovskaia[1]✉ & Jennifer J. Trowbridge[1,2]✉

Oncostatin M (OSM) is a member of the interleukin-6 (IL-6) family of cytokines and has been found to have anti-inflammatory and pro-inflammatory properties in various cellular and disease contexts. OSM signals through two receptor complexes, one of which includes OSMRβ. Here, we investigated OSM-OSMRβ signaling in adult mouse hematopoietic stem cells (HSCs) using the conditional *Osmr*$^{fl/fl}$ mouse model B6;129-*Osmr*$^{tm1.1Nat}$/J. We crossed *Osmr*$^{fl/fl}$ mice to interferon-inducible Mx1-Cre, which is robustly induced in adult HSCs. From these mice, we isolated HSCs by flow cytometry, stimulated with recombinant OSM or vehicle for 1 hour, and assessed gene expression changes in control versus *Osmr* knockout HSCs by RNA-seq. This data may be utilized to investigate OSMRβ -dependent and -independent OSM signaling as well as the transcriptional effects of an IL-6 family cytokine on mouse HSCs to further define its anti-inflammatory versus pro-inflammatory properties.

Background & Summary

OSM plays an important role in development, malignancy, and homeostasis of various tissue types[1–5]. OSM is primarily produced by mature activated hematopoietic cells such as monocytes, T lymphocytes, neutrophils, macrophages, and dendritic cells[4,6,7]. OSM was first isolated based on its ability to inhibit the proliferation of melanoma tumor cells, while having no significant effect on normal human fibroblasts[6]. Despite this initial identification of OSM as a tumor suppressor, a pro-inflammatory role for OSM has subsequently been reported in several solid tumors, myeloma, and chronic lymphocytic leukemia[1,3,8].

Human OSM interacts with two distinct receptor complexes. The type I receptor complex contains leukemia inhibitory factor receptor alpha (LIFR) and interleukin 6 signal transducer (IL6ST; GP130), while the type II receptor complex contains oncostatin M receptor (OSMRβ) and IL6ST[4,9–11]. While recent studies have shown that OSM has a lower affinity for the type I receptor complex than the type II receptor complex[12,13], much remains unknown about how OSM interacts with these complexes in different contexts. While human OSM is known to signal through both the type I and type II receptor complexes, mouse OSM is reported to signal only through the type II receptor complex[14–16]. With respect to hematopoiesis, increased transcript levels of OSMRβ (*Osmr*) are a significant alteration in mouse HSC aging[17,18], prompting us to query the molecular consequences of OSM signaling on HSCs and the extent to which this is dependent on OSMRβ. Thus, we obtained a B6;129-*Osmr*$^{tm1.1Nat}$/J (referred to as *Osmr*$^{fl/fl}$) mouse model and crossed these mice to an interferon-inducible *Mx1*-Cre allele[19], which is commonly used in the study of adult hematopoiesis and also acts with variable efficiency in other tissues. From these mice and their *Mx1*-Cre control counterparts, we prospectively isolated HSCs by flow cytometry, stimulated HSCs *in vitro* with recombinant murine OSM (500 ng/ml) or vehicle for 1 hour and assessed gene expression by RNA-seq (Fig. 1). This RNA-seq data may be used to investigate OSMRβ -dependent and -independent OSM signaling as well as the transcriptional effects of an IL-6 family cytokine on mouse HSCs to further define its anti-inflammatory versus pro-inflammatory properties.

[1]The Jackson Laboratory, Bar Harbor, ME, USA. [2]School of Graduate Biomedical Sciences, Tufts University School of Medicine, Boston, MA, USA. ✉e-mail: maria.telpoukhovskaia@jax.org; Jennifer.trowbridge@jax.org

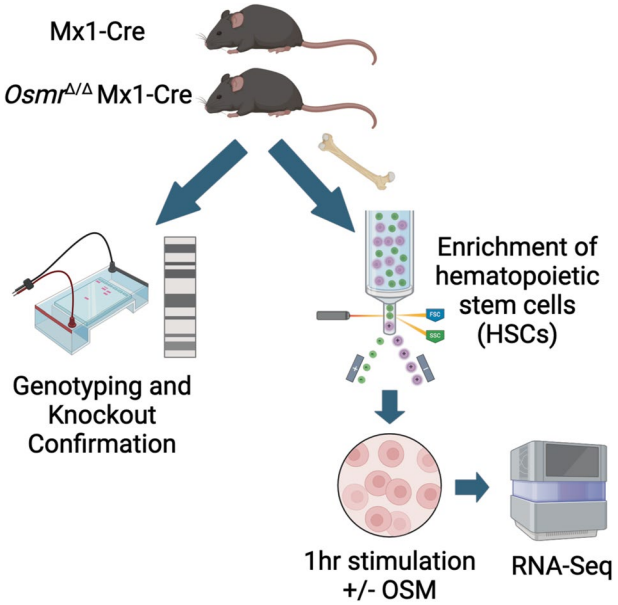

Fig. 1 Overview of the study design and experimental workflow. RNA-seq data was generated from hematopoietic stem cells (HSCs) isolated from control Mx1-Cre and experimental *Osmr*$^{\Delta/\Delta}$ Mx1-Cre mice that had been treated *ex vivo* for 1 hour with recombinant murine OSM (500 ng/ml) or vehicle control[20]. An independent cohort of mice was used for technical validation of the genotype and recombination of *Osmr*$^{\Delta/\Delta}$ Mx1-Cre as well as validation of reduced OSMRβ expression by Western blotting. Created with BioRender.com.

Methods

Mice. C57BL/6 J (JAX:000664) mice were obtained from The Jackson Laboratory. B6;129-*Osmr*$^{tm1.1Nat}$/J (JAX: 011081) were crossed to B6.Cg-Tg(*Mx1*-cre)1Cgn/J mice (JAX:003556). To induce *Mx1*-Cre, mice were intraperitoneally injected once every other day for five total injections with 15 mg/kg high molecular weight polyinosinic-polycytidylic acid (polyI:C) (InvivoGen). Mice used for experiments were young female adults (2–4 months of age) and were used >10 weeks after polyI:C administration. The Jackson Laboratory's Institutional Animal Care and Use Committee approved all experiments.

Genotyping and recombination PCR. Genomic DNA was extracted from lysed peripheral blood samples using the DNeasy Blood & Tissue Kit (Qiagen) for genotyping. Genotyping primers were used as suggested on the B6;129-*Osmr*$^{tm1.1Nat}$/J (JAX: 011081) mice webpage (protocol ID 29086 and 23692). Images were taken using the InGenuis LHR2 Gel imaging system (Syngene). Recombination of the *Osmr*^{fl} locus was evaluated by PCR using the following primers: Forward: 5'-GGAAATACCTTGGCAGTGGTG and Reverse: 5'-GCTACCAAACCTCGGTAATCC.

Western blotting. Total protein was extracted from snap frozen tissues with a Tissue Lyser II (Qiagen) using 5 mm Bead Beater balls (Qiagen) after the addition of 50 mM HEPES pH 7.5 (Gibco) and 6 M urea (Sigma Aldrich) at 1.5 mL per 200 mg tissue. Insoluble material was spun out at 21,000 × g for 20 m. Total protein concentration of each sample was determined by microBCA (ThermoFisher). SDS-PAGE gel samples were prepared. Two 4–15% Mini-PROTEAN TGX Precast, 1.0 mm, 15-well, SDS-PAGE Gel (BioRad) were loaded with 25 ug total protein per well. The gels were run at 150 V for 1 h at room temperature in Tris·Glycine·SDS buffer (BioRad) then transferred overnight at 4 °C at 40 mAmp to 0.22 mm PVDF (BioRad) in Tris·Glycine buffer (BioRad) with 10% methanol. The blots were placed in Block (2% BSA + 4% Dry Milk) at room temperature for 1 h. The blots were then placed in primary antibody Polyclonal Goat IgG anti-mouse OSMRβ (R&D systems AF662) diluted in fresh block at 1:2500 and incubated on an orbital shaker at 4 °C overnight. Then the blots were washed with TBS with 0.03% Tween 20 (TBS-T) for 15 min and three more washes for 5 minutes each. Then the blots were placed in Peroxidase AffiniPure Bovine Anti-Goat IgG (H + L) (Jackson Immuno Research) diluted 1:5,000 in block. The blots rotated for 1 h at room temperature and then were washed with TBS-T for 15 min and three more washes for 5 minutes each. The blot was then developed with (ThermoFisher) SuperSignal West Pico Plus reagents (ThermoFisher) and visualized with a Syngene G-Box. The blots were then stripped with Restore™ PLUS Western Blot Stripping Buffer (ThermoFisher) at room temperature for 5 min. The blots were re-blocked and then incubated with anti-β-actin (Cell Signaling Technology clone D6A8) at 1:5000 for 1 h at room temperature. Then the blots were washed with TBS-T for 15 min and three more washes for 5 minutes each. Then the blots were placed in Goat Anti-Rabbit IgG (H + L)-HRP (Bio-Rad) diluted 1:5,000 in block. The blots rotated for 1 h at room temperature and then were washed with TBS-T for 15 min and three more washes for 5 minutes each. The blot was then developed with SuperSignal West Femto Maximum Sensitivity reagents (ThermoFisher) and visualized with a Syngene G-Box. Images were quantified by ImageJ by relative intensity, adjusted for background

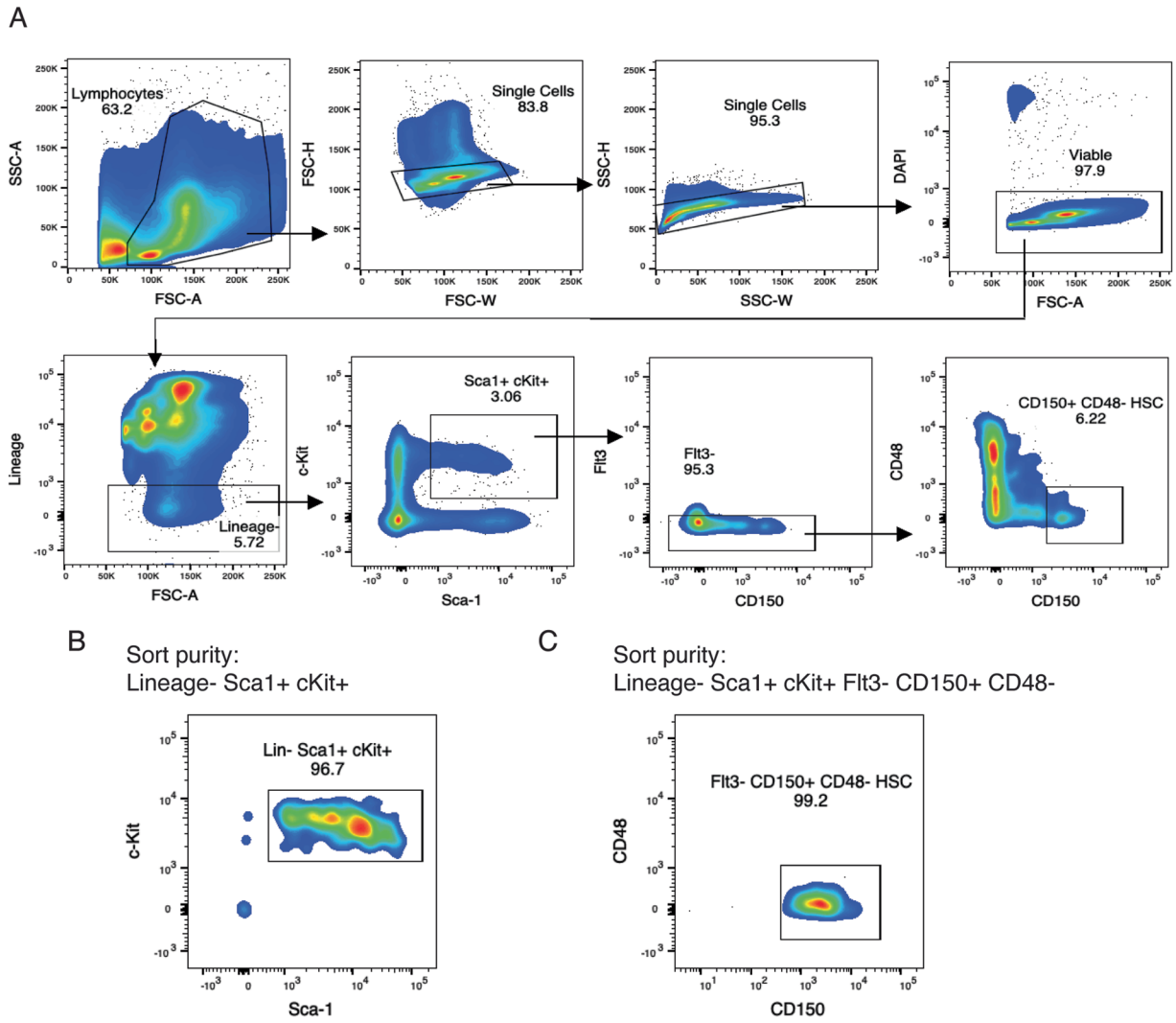

Fig. 2 Cell sorting plots and purity for control *Mx1*-Cre and $Osmr^{\Delta/\Delta}$ *Mx1*-Cre HSCs. (**A**) Representative flow cytometric gating used for isolation of HSCs as viable Lin- Sca-1+ c-Kit+Flt3- CD150+ CD48- cells. (**B**) Representative purity of isolated Lin- Sca-1+ c-Kit+ HSPCs after cell sorting, which was >95%. (**C**) Representative purity of isolated Lin- Sca-1+ c-Kit + Flt3- CD150+ CD48- HSCs after cell sorting, which was >99%.

and normalized to β-Actin expression per sample. Significance was calculated using paired *t* test with correction for multiple comparisons using the Holm-Sidak method. Calculation of significance and graphing was performed using Prism 10 (GraphPad).

RNA sequencing. Bone marrow (BM) cells were isolated from $Osmr^{\Delta/\Delta}$ *Mx1*-Cre and *Mx1*-Cre from pooled and crushed femurs, tibiae, iliac crests, sternums, forepaws, and spinal columns of individual mice. BM mononuclear cells (MNCs) were isolated by 1X Red Blood Cell lysis Buffer (eBioscience) and stained with a panel of fluorochrome-conjugated antibodies against c-Kit (BD Biosciences, BioLegend clone 2B8), Sca-1 (BioLegend clone D7), CD150 (BioLegend clone TC15-12F12.2), CD48 (BioLegend clone HM48-1), FLT3 (BioLegend clone A2F10), (Lin) marker mix (B220 (BD Biosciences, BioLegend clone RA3-6B2), and 4′,6-diamidino-2-phenylindole (DAPI). 2,000 hematopoietic stem cells (HSCs) were prospectively isolated based on the cell surface marker combination: Lin- Sca-1+ c-Kit+ Flt3- CD150+ CD48- on a FACSAria with >95% purity (Fig. 2). HSCs were directly sorted into StemSpan SFEM II media with SCF (100 ng/ml, BioLegend), TPO (50 ng/ml, Peprotech), with or without OSM (500 ng/ml, BioLegend) and incubated at 37 °C for 60 min. Cells were then washed, pelleted and flash frozen. Total RNA was isolated from flash-frozen pellets using the RNeasy Micro Kit (Qiagen) including the optional DNase digest step. RNA concentration and quality were assessed using the RNA 6000 Pico Assay (Agilent Technologies). Libraries were constructed using the SMARTer Stranded Total RNA-Seq Kit v2-Pico (Takara) according to the manufacturer's protocol. Library concentration and quality were assessed using the D5000 ScreenTape (Agilent Technologies) and Qubit dsDNA HS Assay (ThermoFisher). Libraries were subject to 75 bp paired-end sequencing on an Illumina NextSeq 500 using

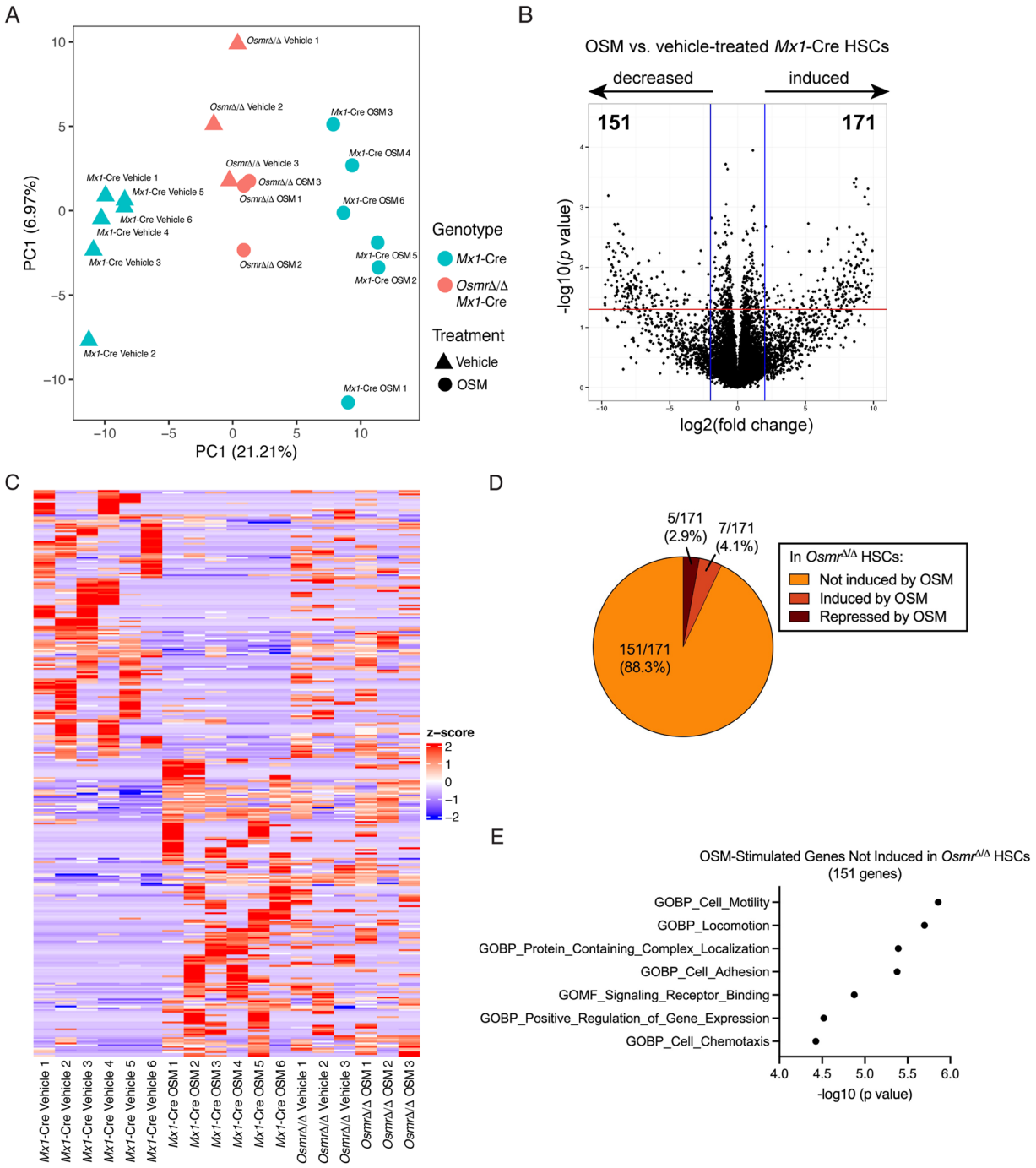

Fig. 3 Differential gene expression analysis of recombinant OSM-stimulated genes in control *Mx1*-Cre and *Osmr*$^{\Delta/\Delta}$ *Mx1*-Cre HSCs. (**A**) Principal component analysis of all biological replicate samples of control *Mx1*-Cre HSCs treated with OSM ($n = 6$) or without OSM ($n = 6$) and *Osmr*$^{\Delta/\Delta}$ *Mx1*-Cre HSCs treated with OSM ($n = 3$) or without OSM ($n = 3$)[20]. (**B**) Volcano plot showing differential gene expression of OSM-treated vs. vehicle-treated control *Mx1*-Cre HSCs. Numbers of significantly differentially expressed genes (log2(FC) >2 or <-2, $p < 0.05$) are indicated. See also Supplementary Table 2. (**C**) Heatmap of gene expression across all samples of the 322 differentially expressed genes identified in OSM-treated vs. vehicle-treated control *Mx1*-Cre HSCs. (**D**) Proportions of the 171 OSM-induced genes in Mx1-Cre HSCs assessed in OSM-treated vs. vehicle-treated *Osmr*$^{\Delta/\Delta}$ Mx1-Cre HSCs. Cutoff for significantly induced or repressed genes utilized $p < 0.05$ criteria. See also Supplementary Table 3. (**E**) Gene ontology (GO) term enrichment of 151 OSM-induced genes in control *Mx1*-Cre HSCs that were not induced by OSM in *Osmr*$^{\Delta/\Delta}$ Mx1-Cre HSCs.

the High Output Reagent Kit v2.5 or 150 bp paired-end on an Illumina NovaSeq 6000 using the S4 Reagent Kit v1.5. Trimmed alignment files were processed using RSEM (v1.3.3 or v1.3.1). Alignment to the mm10 reference genome was completed using Bowtie 2 (v2.4.1 or v2.4.5). Expected read counts per gene produced by RSEM

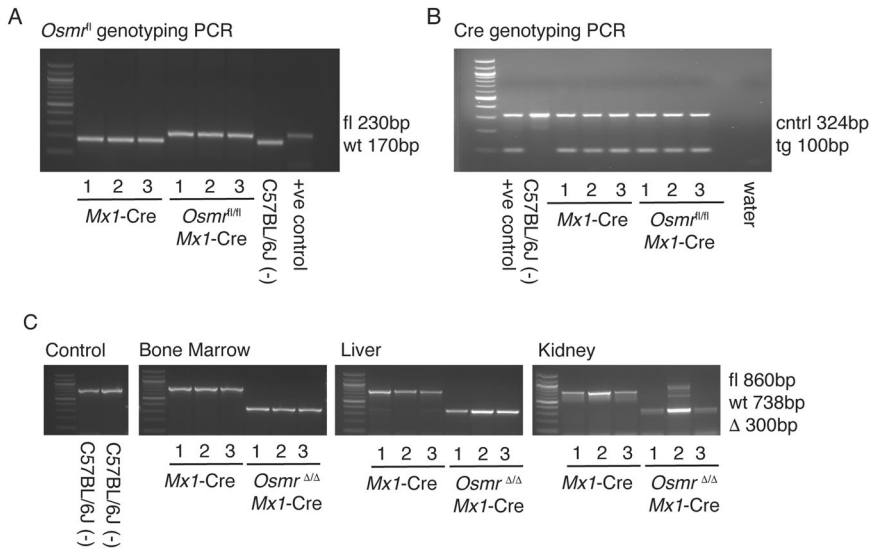

Fig. 4 Genotyping and recombination of the *Osmr*^{fl} locus in tissues from *Osmr*$^{\Delta/\Delta}$ Mx1-Cre mice. Agarose gel electrophoresis (2% agarose) of PCR-amplified products. In all gels a 100 bp ladder was used for size estimation located in lane 0. (**A**) Genotyping PCR for Osmr <tm1.1Nat> from ear punch genomic DNA. Lanes 1–3 are from Mx1-Cre mice, lanes 4–6 are from *Osmr*$^{fl/fl}$ Mx1-Cre mice, lane 7 is from a wild-type C57BL/6 J mouse and lane 8 is from a positive control *Osmr*$^{fl/fl}$ confirmed by The Jackson Laboratory's in-house genotyping service. (**B**) Genotyping PCR for Cre recombinase from ear punch genomic DNA. Lane 1 is from a positive control, lane 2 is from a wild-type C57BL/6 J mouse, lanes 3–5 are from Mx1-Cre mice and lanes 6–8 are from *Osmr*$^{fl/fl}$ Mx1-Cre mice. (**C**) Recombination PCR for the Osmr <tm1.1Nat> allele from indicated tissues. From left, lanes 1–2 are from blood samples from wild-type C57BL/6 J mice. In the remaining images, samples are ordered as lanes 1–3 from Mx1-Cre mice and lanes 4–6 from *Osmr*$^{\Delta/\Delta}$ Mx1-Cre mice.

were rounded to integer values. Filtered total read counts had an average of 151 million counts (±32 million standard deviation), Q30 rate of 93% (±1% standard deviation), 52% GC rate (±2% standard deviation), and 28 million (±9 million standard deviation) read pairs mapped to genes (Table S1, see supplementary xlsx file). Counts were filtered to include only genes that had at least two samples within a sample group having a counts per million reads >1 in R (v4.1.3), and edgeR (v3.36.0) was used for differential expression analysis. A negative binomial generalized log-linear model was fit to the read counts for each gene. The dispersion trend was estimated by Cox-Reid approximate profile likelihood followed by empirical Bayes estimate of the negative binomial dispersion parameter for each tag, with expression levels specified by a log-linear model. Likelihood ratio tests for coefficient contrasts in the linear model were evaluated producing a p value per contrast. The Benjamini and Hochberg's algorithm was used to control the false discovery rate. Features with fold change (FC) >2 or <−2 and $p < 0.05$ were declared significantly differentially expressed. Predicted genes and pseudogenes were removed from the list of significantly differentially expressed genes before downstream comparisons were performed.

Data Records

The RNA-seq dataset is available at the Gene Expression Omnibus (GEO) [GSE244544[20]], with this section being the primary source of information on the availability and content of the data being described. This dataset includes a total of 18 RNA-seq samples. The first group of samples are control *Mx1*-Cre HSCs treated for 1 hour with vehicle ($n = 6$, filenames: GSM7818933 Mx1-Cre Veh 1, GSM7818934 Mx1-Cre Veh 2, GSM7818935 Mx1-Cre Veh 3, GSM7818936 Mx1-Cre Veh 4, GSM7818937 Mx1-Cre Veh 5, GSM7818938 Mx1-Cre Veh 6)[20]. The second group of samples are control *Mx1*-Cre HSCs treated for 1 hour with 500 ng/ml OSM ($n = 6$, filenames: GSM7818939 Mx1-Cre OSM 1, GSM7818940 Mx1-Cre OSM 2, GSM7818941 Mx1-Cre OSM 3, GSM7818942 Mx1-Cre OSM 4, GSM7818943 Mx1-Cre OSM 5, GSM7818944 Mx1-Cre OSM 6)[20]. The third group of samples are *Osmr*$^{\Delta/\Delta}$ *Mx1*-Cre HSCs treated for 1 hour with vehicle ($n = 3$, filenames: GSM7818927 Osmrfl/fl Mx1-Cre Veh 1, GSM7818928 Osmrfl/fl Mx1-Cre Veh 2, GSM7818929 Osmrfl/fl Mx1-Cre Veh 3)[20]. The fourth group of samples are *Osmr*$^{\Delta/\Delta}$ *Mx1*-Cre HSCs treated for 1 hour with 500 ng/ml OSM ($n = 3$, filenames: GSM7818930 Osmrfl/fl Mx1-Cre OSM 1, GSM7818931 Osmrfl/fl Mx1-Cre OSM 2, GSM7818932 Osmrfl/fl Mx1-Cre OSM 3)[20].

We utilized this dataset to explore how control *Mx1*-Cre versus *Osmr*$^{\Delta/\Delta}$ *Mx1*-Cre HSCs respond to stimulation with recombinant murine OSM. First, we performed principal component analysis to cluster control *Mx1*-Cre and *Osmr*$^{\Delta/\Delta}$ *Mx1*-Cre HSCs treated with or without OSM[20] (Fig. 3A). We observed that OSM-treated versus vehicle-treated control HSCs clearly separated on principal component 1 (PC1) whereas OSM-treated versus vehicle treated *Osmr*$^{\Delta/\Delta}$ HSCs did not separate on PC1 and were partially separated on PC2, indicating

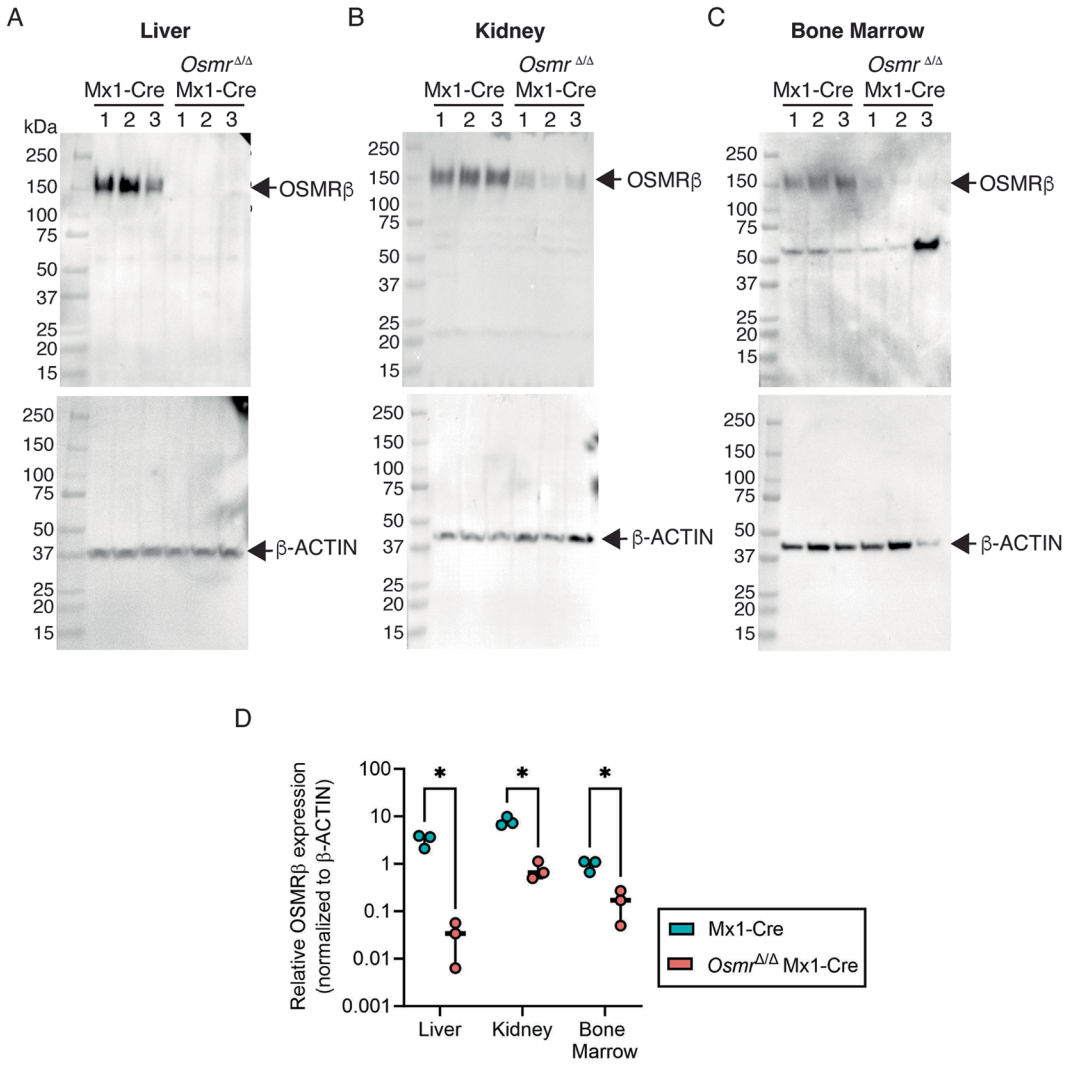

Fig. 5 Assessment of OSMRβ in tissues from *Osmr*$^{\Delta/\Delta}$ Mx1-Cre mice. (**A–C**) Western blot analysis of cell lysates from (**A**) liver, (**B**) kidney, and (**C**) bone marrow from Mx1-Cre and *Osmr*$^{\Delta/\Delta}$ Mx1-Cre mice. Blots were probed with antibodies against OSMRβ (~150 kDa) and β-ACTIN (45 kDa) ($n = 3$ biological replicates per genotype). (**D**) Relative protein expression assessed by Western blot imaging using ImageJ. OSMRβ band densities were normalized to β-ACTIN. Dots represent individual mice. *$p < 0.05$. Significance was calculated using paired *t* test with *p* values adjusted for multiple comparisons using the Holm-Sidak method.

greater transcriptional changes in control HSCs is response to OSM compared to *Osmr*$^{\Delta/\Delta}$ HSCs in response to OSM. Using the cutoffs for significance defined above, control HSCs had 171 genes increased in expression following OSM stimulation compared to vehicle treatment and 151 genes decreased in expression following OSM stimulation (Fig. 3B, Table S2, Table S3, see supplementary xlsx files). These differentially expressed genes were observed across biological replicate samples (Fig. 3C). Focusing on the 171 genes induced by OSM in control HSCs, we examined their expression in *Osmr*$^{\Delta/\Delta}$ HSCs (Table S4). This revealed several patterns: 151 of these genes (88.3%) were no longer induced by OSM in *Osmr*$^{\Delta/\Delta}$ HSCs, 7 genes (4.1%) were induced by OSM in both control and *Osmr*$^{\Delta/\Delta}$ HSCs, and 5 genes (2.9%) were induced by OSM in control HSCs but repressed by OSM in *Osmr*$^{\Delta/\Delta}$ HSCs (Fig. 3D). We then analyzed the 151 genes induced by OSM stimulation in control HSCs but no longer induced in *Osmr*$^{\Delta/\Delta}$ HSCs using the molecular signatures database (MSigDB)[21] focused on gene ontology (GO) terms. This analysis revealed enrichment of GO terms including cell motility, protein containing complex localization, cell adhesion, signaling receptor binding and positive regulation of gene expression (Fig. 3E).

Technical Validation

Verification of genotype and *osmr*$^{tm1.1Nat}$ allele recombination. After crossing B6;129-*Osmr*$^{tm1.1Nat}$/J to Mx1-Cre to generate *Osmr*$^{fl/fl}$ Mx1-Cre and control Mx1-Cre animals, we genotyped three control and three experimental animals alongside positive (parental *Osmr*$^{fl/fl}$ and *Mx1*-Cre mice) and negative (wild-type C57BL/6 J) controls. At the *Osmr* locus, genomic DNA from *Osmr*$^{fl/fl}$ Mx1-Cre mice contained a loxP site (230 bp) and genomic DNA from control Mx1-Cre mice did not contain a loxP site (170 bp), recognized by primers flanking exon 2 (Fig. 4A). Genomic DNA from all *Osmr*$^{fl/fl}$ Mx1-Cre and control Mx1-Cre mice were also positive

for the transgenic cre allele (100 bp) (Fig. 4B). Following injection with poly(I:C) to induce Mx1-Cre-mediated recombination of the *Osmr*^{fl} locus, we isolated DNA from bone marrow, liver, and kidney tissues. A recombination PCR assay was designed to assess *Osmr*^{fl} recombination efficiency. The primers generate a product spanning the loxP-flanked exon 2 and bind to both the wild-type and modified *Osmr* loci generating product sizes of ~860 bp for the floxed (fl) allele, 738 bp for the wild-type (wt) allele and ~300 bp for the recombined (Δ) allele. This PCR assay detected a ~300 bp recombined allele in all tissue samples from *Osmr*$^{\Delta/\Delta}$ mice (Fig. 4C), demonstrating that recombination of the *Osmr* locus occurred efficiently following poly(I:C) injection in the bone marrow, liver, and kidney.

Confirmation of OSMRβ knockout. We performed western blotting with a published murine OSMRβ antibody[12,14,22,23] to evaluate protein expression in the liver, kidney, and bone marrow isolated from *Osmr*$^{\Delta/\Delta}$ and control mice. OSMRβ in the liver was undetectable in *Osmr*$^{\Delta/\Delta}$ mice (Fig. 5A) and OSMRβ expression in the kidney and bone marrow were reduced to very low levels in *Osmr*$^{\Delta/\Delta}$ mice (Fig. 5B,C). Quantitation of bands by relative intensity using ImageJ determined that OSMRβ was significantly reduced in *Osmr*$^{\Delta/\Delta}$ compared to control mouse liver, kidney, and bone marrow, respectively (Fig. 5D). Due to the variable efficiency in *Mx1*-Cre-mediated deletion across tissues, OSMRβ expression may be retained on certain cells, accounting for differences between the data presented in Figs. 4 and 5.

Code availability

No custom code was generated or used for analysis of the data presented.

Received: 19 February 2024; Accepted: 28 August 2024;
Published online: 12 September 2024

References

1. Masjedi, A. *et al*. Oncostatin M: A mysterious cytokine in cancers. *Int Immunopharmacol* **90**, 107158, https://doi.org/10.1016/j.intimp.2020.107158 (2021).
2. Houben, E., Hellings, N. & Broux, B. Oncostatin M, an Underestimated Player in the Central Nervous System. *Front Immunol* **10**, 1165, https://doi.org/10.3389/fimmu.2019.01165 (2019).
3. Chen, M. *et al*. Exploring the oncostatin M (OSM) feed-forward signaling of glioblastoma via STAT3 in pan-cancer analysis. *Cancer Cell Int* **21**, 565, https://doi.org/10.1186/s12935-021-02260-9 (2021).
4. Tanaka, M. & Miyajima, A. Oncostatin M, a multifunctional cytokine. *Rev Physiol Biochem Pharmacol* **149**, 39–52, https://doi.org/10.1007/s10254-003-0013-1 (2003).
5. Stephens, J. M. & Elks, C. M. Oncostatin M: Potential Implications for Malignancy and Metabolism. *Curr Pharm Des* **23**, 3645–3657, https://doi.org/10.2174/1381612823666170704122559 (2017).
6. Zarling, J. M. *et al*. Oncostatin M: a growth regulator produced by differentiated histiocytic lymphoma cells. *Proc Natl Acad Sci USA* **83**, 9739–9743, https://doi.org/10.1073/pnas.83.24.9739 (1986).
7. Malik, N. *et al*. Molecular cloning, sequence analysis, and functional expression of a novel growth regulator, oncostatin M. *Mol Cell Biol* **9**, 2847–2853, https://doi.org/10.1128/mcb.9.7.2847-2853.1989 (1989).
8. Araujo, A. M. *et al*. Stromal oncostatin M cytokine promotes breast cancer progression by reprogramming the tumor microenvironment. *J Clin Invest* **132**, https://doi.org/10.1172/JCI148667 (2022).
9. Auguste, P. *et al*. Signaling of type II oncostatin M receptor. *J Biol Chem* **272**, 15760–15764, https://doi.org/10.1074/jbc.272.25.15760 (1997).
10. Mosley, B. *et al*. Dual oncostatin M (OSM) receptors. Cloning and characterization of an alternative signaling subunit conferring OSM-specific receptor activation. *J Biol Chem* **271**, 32635–32643, https://doi.org/10.1074/jbc.271.51.32635 (1996).
11. Gearing, D. P. *et al*. The IL-6 signal transducer, gp130: an oncostatin M receptor and affinity converter for the LIF receptor. *Science* **255**, 1434–1437, https://doi.org/10.1126/science.1542794 (1992).
12. Walker, E. C. *et al*. Oncostatin M promotes bone formation independently of resorption when signaling through leukemia inhibitory factor receptor in mice. *J Clin Invest* **120**, 582–592, https://doi.org/10.1172/JCI40568 (2010).
13. Sims, N. A. Influences of the IL-6 cytokine family on bone structure and function. *Cytokine* **146**, 155655, https://doi.org/10.1016/j.cyto.2021.155655 (2021).
14. Adrian-Segarra, J. M. *et al*. The AB loop of oncostatin M (OSM) determines species-specific signaling in humans and mice. *J Biol Chem* **293**, 20181–20199, https://doi.org/10.1074/jbc.RA118.004375 (2018).
15. Drechsler, J., Grotzinger, J. & Hermanns, H. M. Characterization of the rat oncostatin M receptor complex which resembles the human, but differs from the murine cytokine receptor. *PLoS One* **7**, e43155, https://doi.org/10.1371/journal.pone.0043155 (2012).
16. Ichihara, M., Hara, T., Kim, H., Murate, T. & Miyajima, A. Oncostatin M and leukemia inhibitory factor do not use the same functional receptor in mice. *Blood* **90**, 165–173 (1997).
17. Flohr Svendsen, A. *et al*. A comprehensive transcriptome signature of murine hematopoietic stem cell aging. *Blood* **138**, 439–451, https://doi.org/10.1182/blood.2020009729 (2021).
18. Sempowski, G. D. *et al*. Leukemia inhibitory factor, oncostatin M, IL-6, and stem cell factor mRNA expression in human thymus increases with age and is associated with thymic atrophy. *J Immunol* **164**, 2180–2187, https://doi.org/10.4049/jimmunol.164.4.2180 (2000).
19. Kuhn, R., Schwenk, F., Aguet, M. & Rajewsky, K. Inducible gene targeting in mice. *Science* **269**, 1427–1429, https://doi.org/10.1126/science.7660125 (1995).
20. Schwartz, L. S., Stearns, T., Trowbridge, J. J. & Telpoukhovskaia, M., GEO. https://identifiers.org/geo/GSE244544 (2024).
21. Subramanian, A. *et al*. Gene set enrichment analysis: a knowledge-based approach for interpreting genome-wide expression profiles. *Proc Natl Acad Sci USA* **102**, 15545–15550, https://doi.org/10.1073/pnas.0506580102 (2005).
22. Wang, E. C. E., Dai, Z., Ferrante, A. W., Drake, C. G. & Christiano, A. M. A Subset of TREM2(+) Dermal Macrophages Secretes Oncostatin M to Maintain Hair Follicle Stem Cell Quiescence and Inhibit Hair Growth. *Cell Stem Cell* **24**, 654–669 e656, https://doi.org/10.1016/j.stem.2019.01.011 (2019).
23. Bisht, K. *et al*. Oncostatin M regulates hematopoietic stem cell (HSC) niches in the bone marrow to restrict HSC mobilization. *Leukemia* **36**, 333–347, https://doi.org/10.1038/s41375-021-01413-z (2022).

Acknowledgements
This work was supported by National Institutes of Health grants R01DK118072, R01AG069010, U01AG077925, and a Discovery Research Grant from the Edward P. Evans Foundation to J.J.T. This work was supported in part by the NIH/NCI Cancer Center Support Grant P30CA034196. J.J.T. was supported by a Leukemia & Lymphoma Society Scholar Award and The Dattels Family Endowed Chair. L.S.S. was supported by F31DK127573 and The Tufts University Scheer-Tomasso Fund philanthropic gift. We thank Drs. Jeremy Nathans and Amir Rattner for providing detailed information regarding the design of the B6;129-*Osmr*$^{tm1.1Nat}$/J allele. We thank all members of the Trowbridge Lab for experimental support and manuscript editing. We thank the Scientific Services at The Jackson Laboratory including flow cytometry and genome technologies. We thank Elli Hartig, Carol Bult, Ryan Tewhey, Cliff Rosen, and Phil Hinds for their input.

Author contributions
L.S.S. conceptualized the project, designed experiments, performed experiments, analyzed data, uploaded the RNA-seq data to the GEO repository, and wrote the manuscript. R.L.S. optimized and performed Western blotting and image analysis and edited the manuscript. T.S. analyzed the RNA-seq data and edited the manuscript. M.T. compiled and analyzed the RNA-seq data, generated figure panels, edited records in the GEO repository, and wrote the manuscript. J.J.T. conceptualized the project, designed experiments, analyzed data, and wrote the manuscript.

Competing interests
J.J.T. has previously received research support from H3 Biomedicine, Inc., and patent royalties from Fate Therapeutics.

Additional information
Supplementary information The online version contains supplementary material available at https://doi.org/10.1038/s41597-024-03839-3.

Correspondence and requests for materials should be addressed to M.T. or J.J.T.